Early Stage Quiescent and Flow-Induced Crystallization of Intercalated Polypropylene Nanocomposites by Time-Resolved Light Scattering

Anongnat Somwangthanaroj,[†] Ellen C. Lee,[‡] and Michael J. Solomon*,[†,§]

Macromolecular Science and Engineering Program and Department of Chemical Engineering, University of Michigan, Ann Arbor, Michigan 48109, and Scientific Research Labs, Ford Motor Company, Dearborn, Michigan 48124

ABSTRACT: Time-resolved light scattering demonstrates that the early-stage quiescent and flow-induced crystallization kinetics of an intercalated polypropylene clay nanocomposite differs significantly from that of pure polypropylene. The material studied is organophilic montmorillonite clay dispersed at 2.0 wt % by melt mixing in an isotactic polypropylene matrix with maleic anhydride functionalized polypropylene compatibilizer. Characteristic crystallization times are extracted from the time evolution of integral measures of the angularly dependent parallel polarized and cross polarized light scattering intensity. For quiescent isothermal crystallization with undercooling $\Delta T < 32$ °C, measured relative to its melting temperature, the compatibilized, intercalated nanocomposite displays retarded crystallization kinetics compared to that of pure polypropylene. However, the nanocomposite behavior does not differ significantly from that of a polypropylene/maleic anhydride functionalized polypropylene blend within the temperature range for which the characteristic crystallization times of the latter material could be extracted. Debye−Bueche analysis of the polarized light scattering intensity demonstrates significant differences in the time-dependent growth of isotropic morphology in the polymer and the nanocomposite. Marked flow-induced acceleration of crystallization kinetics is observed for the polymer nanocomposite at applied strain rates for which flow has only a modest effect on polypropylene crystallization. By comparing this behavior to that of a blend of polypropylene and compatibilizer, we infer a significant role for the latter species in flow-induced nanocomposite crystallization. We furthermore find that the magnitude of the flow-induced acceleration of crystallization for the polypropylene nanocomposite is a unique function of the applied strain.

Introduction

Dilute concentrations of organophilic swelling clays dispersed in a polymer matrix have unusual and valuable mechanical, thermal, and permeability properties relative to the pure polymer.[1] The effect of clay on these properties is significant if the clay has an intercalated tactoid structure. Alternatively, exfoliated materials, in which the clay is dispersed at the level of individual platelets, are thought to provide even greater potential for material property enhancement. Such polymer/clay nanocomposites have been prepared for a broad range of matrix polymers, as described in a recent review[1] and the citations therein. Nanocomposites produced with nylon-6 or polypropylene are of particular interest because of their commercial applicability. By the addition of swelling clays, significant enhancement in the solid-state tensile modulus and tensile strength has been reported for these materials,[2−5] even for those cases where intercalated tactoid structure was evident.[3,4]

It is remarkable that the addition of just a few percent by weight of clay can result in significant mechanical property enhancement, and thus elucidation of the mechanism of enhancement is of particular interest. Micromechanical composite models[6,7] are one possible avenue by which this enhancement may be investigated. Here we take an alternative approach by investigating the hypothesis that clay particles affect the crystalline morphology of the polymer, thereby mediating an enhancement in solid-state mechanical properties. This hypothesis is supported by recent observations that addition of clay to nylon-6 can result, at particular cooling rates, in a switch in crystal form from the α to the γ phase.[8] Other possible effects, such as a change in the degree of crystallinity or secondary structure, might also be linked to changes in mechanical properties such as strength and yield.[9] Moreover, mechanistically, clay might affect polymer crystallization by promoting nucleation. Finally, crystallite growth rates and secondary morphology could be affected by the percolated structure of the clay tactoids and dispersed platelets.

These possible mechanisms can be studied by comparing the crystallization kinetics of pure polymer and polymer nanocomposite. Investigation of the early stages of crystallization is of particular interest, because of the possible role of clay platelets and tactoids in crystal nucleation. Polymer crystallization kinetics have been studied by means of differential scanning calorimetry, optical microscopy, rheology, and light or X-ray scattering.[10,11] These methods, with varying sensitivity, probe different length scales of the material and/or time scales of the crystallization process.[12] Recent studies have demonstrated that time-resolved, polarization-dependent light scattering is particularly sensitive to micron scale density and orientation fluctuations that accompany the earliest stages of polymer crystallization.[12−15] For this reason, here we apply light scattering to study the effect of clay platelets on polymer crystallization. We are aided in this endeavor by powerful classical theory[16−21] that allows the quantitative interpretation of polarization-dependent light scattering in

[†] Macromolecular Science and Engineering Program, University of Michigan.
[‡] Ford Motor Company.
[§] Department of Chemical Engineering, University of Michigan.

terms of density and orientation fluctuations of the crystallizing polymer. We study isothermal crystallization because of its long history as a model experiment for polymer crystallization.[10]

Commercial applications of polymer nanocomposites will likely involve processing operations such as injection and compression molding. In these cases the flow applied during processing could play a decisive role in crystallization kinetics and the resultant morphology formed. For example, studies of the flow-induced crystallization have demonstrated that flow accelerates crystallization kinetics according to mechanisms that remain under investigation (cf. refs 10, 14, and 22−34 and citations therein). Analogous studies for polymer/clay nanocomposites are currently lacking. Because of its possibly important role, here we investigate the flow-induced crystallization of nanocomposites and compare the results to parallel studies of quiescent crystallization.

Our work provides information that is complementary to a recent study of the qualitative effect of shear flow on the nonisothermal crystallization of nylon-6 nanocomposites.[35] These authors report in situ small (SAXS) and wide (WAXS) angle X-ray studies of the effect of high strain flow on nylon-6 crystallization. In that work, clay orientation during and after shear was probed by SAXS and polymer nonisothermal crystallization after shear by WAXS. In comparison, polarization-dependent light scattering is sensitive to an earlier stage of crystallization than WAXS.[12] In addition, to decouple flow and thermal effects, we execute experiments in which a short episode of intense shear is followed by isothermal, quiescent crystallization in the way recommended in ref 29. Ex-situ clay orientation in polypropylene nanocomposites subjected to biaxial and uniaxial extensional flow has also recently been characterized.[36,37] Here, we probe polymer crystallization and morphology rather than clay structure and orientation because the light scattering is dominated by the contribution from the growing polymer crystallites.

The intercalated polypropylene nanocomposites used in this study are excellent materials for investigation of quiescent and flow-induced crystallization by time-resolved light scattering for the following reasons: (1) Pure polypropylene has long been a model material for the study of quiescent and flow-induced crystallization. Studies of PP nanocomposites can be fruitfully compared to these literature results; (2) intercalated polypropylene nanocomposites, which show modest solid-state mechanical property enhancement, have numerous possible applications in the packaging, aerospace, and automotive industries. To avoid any possible effects of multiple scattering or residual clay scattering, we study intercalated nanocomposites with low clay loading (no greater than 2.0 wt %). However, note that even at this low particle loading, significant effects of clay on material properties, such as solidlike melt state linear viscoelasticity, have been observed.[38]

The organization of the paper is the following: First, we review material preparation and characterization, describe the light scattering device and experimental protocol, and report the data analysis procedures that allow extraction of early stage crystallization kinetics and morphology. Next, we report and discuss quiescent crystallization studies. Then, we describe the results of our study of flow-induced crystallization. We find sig-
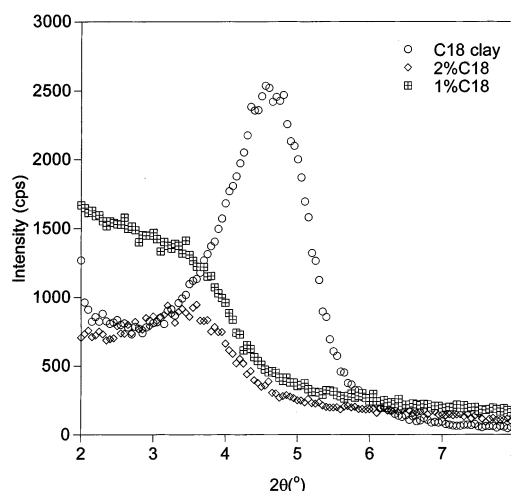

Figure 1. Comparison of ambient temperature wide-angle X-ray scattering of the C-18 amine-exchanged clay and intercalated polypropylene nanocomposites with 1.0 and 2.0 wt % inorganic content prepared by melt mixing.

nificant differences between pure polypropylene and polymer/clay nanocomposites crystallization under both quiescent and flow conditions. We consider the role of the compatibilizer in mediating the observed differences and conclude that it significantly affects the morphology and kinetics of polypropylene nanocomposite crystallization.

Materials and Methods

Materials and Characterization. Intercalated polypropylene nanocomposites were prepared as in Kawasumi et al.[4] and Solomon et al.[38] Briefly, polypropylene was melt mixed with an amine-exchanged montmorillonite and a polypropylene functionalized maleic anhydride compatibilizer. The organophilic clay was produced by ion exchange of a high-purity Na−montmorillonite (Mineral Colloid BP, Southern Clay product, Gonzales, TX, cation exchange capacity (CEC) = 90 ± 1 mequiv/100 g) with the surfactant stearylamine (C-18). Polypropylene (PP31U18A, Equistar Chemicals, M_w = 246 200 g/mol and M_w/M_n = 6.1[38]) and the maleic anhydride functionalized polypropylene compatibilizer (PP-MA) (Polybond 3200, Uniroyal Chemical, M_w = 92 000 g/mol, M_w/M_n = 2.6 and maleic anhydride (MA) content 0.43 wt %[38]) were used as received. Melt mixing (175 °C, 40 min) was performed in a nitrogen environment in a Banbury mixer attached to a Braebender plasticorder. Materials with 1.0 and 2.0 wt % clay were produced. To ameliorate any possible effect of variable PP−MA concentration on crystallization, we deviated from the procedure of refs 4 and 38 by fixing the weight ratio of polypropylene to compatibilizer at 7.28:1 for all samples. For purposes of comparison, a blend of PP and PPMA was also prepared at this same weight ratio.

Thin films (400 μm, by compression molding) of the melt mixed materials were characterized by wide-angle X-ray scattering (WAXS) at ambient temperature on a Rigaku rotating anode diffractometer with Cu Kα radiation of wavelength 1.54 Å. The accelerating voltage was 40 kV. The freeze-dried organophilic clay (C-18) powder was studied for comparison. The WAXS characterization results are reported in Figure 1. The WAXS peaks, which correspond to the {001} basal reflection of the montmorillonite aluminosilicate, are indicative of intercalated structure. Further information regarding WAXS characterization of intercalated polypropylene nanocomposites is available in refs 4 and 38. Note that the lack of a distinct intercalation peak for the 1 wt % nanocomposite is more likely related to instrument sensitivity than the actual presence of exfoliated structure.

To determine the degree of undercooling in light scattering studies, the melting temperature of the materials was esti-
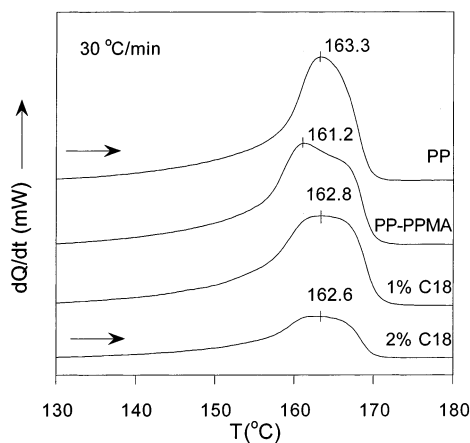
Figure 2. Differential scanning calorimetry endotherms for specimens of pure polypropylene, the blend of PP–PPMA of weight ratio 7.28:1, and intercalated nanocomposites with 1.0 and 2.0 wt % inorganic content.
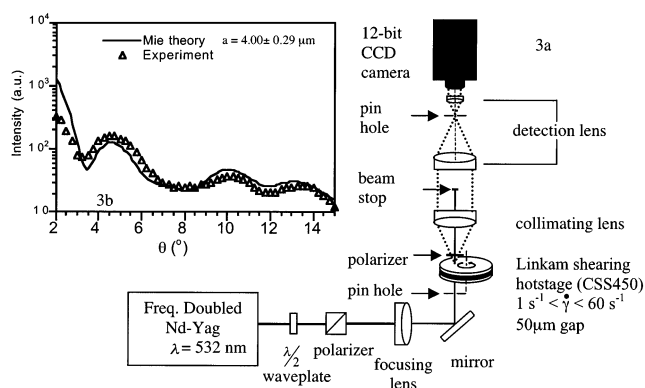

Figure 3. (a) Schematic of the small-angle light scattering apparatus. (b) Measured angular dependence of light scattered for a dilute aqueous solution of polystyrene latex. The performance of the device can be assessed by comparison to calculations by Mie scattering theory.

Figure 4. Temperature and shear history protocols for isothermal crystallization studies.

Figure 5. Depolarized (I_{Hv}) and polarized (I_{Vv}) light scattering patterns measured at different times for quiescent isothermal crystallization of the 2.0 wt % intercalated nanocomposite at $T = 142$ °C.

mated by differential scanning calorimetry (DSC, Perkin-Elmer DSC-6 thermal analyzer) conducted at a scan rate (30 °C/min) that matched the cooling rate of the light scattering experiments. Results are shown in Figure 2. The endothermic curves are normalized to the unit weight of the sample and offset for purposes of comparison. At this cooling rate, the addition of compatibilized organophilic clay to the polypropylene does not significantly affect the melting temperature, which was estimated as the temperature of maximum heat flux, although the nanocomposite peaks are slightly broadened relative to pure PP. Note because its heat flux curve shows multiple endothermic peaks, the PP–PPMA blend displays different crystallization behavior than the other three materials. This behavior is expected for the maleated blend, which may exhibit component immiscibility at low temperatures.[39]

Small-Angle Light Scattering (SALS). A schematic of the device used for SALS is shown in Figure 3a. The design was adapted from Varadan and Solomon[40] to allow the detection of polarization-dependent light scattering. Polarized light from a frequency-doubled Nd:YAG laser (Compass 315M, 150 mW, $\lambda_0 = 0.532$ µm, Coherent Inc., Santa Clara, CA) was variably attenuated by a half-wave plate and a polarizing beam splitter. The polarized light was then steered to and focused at the scattering volume within a temperature-controlled, parallel quartz plate shear cell (CSS 450, Linkham Scientific Instruments Ltd. UK). The light propagated parallel to the gradient direction of the shear cell. (Thus, scattering is detected in the flow–vorticity plane.) The gap between the parallel plates was held fixed at 50 µm (except for experiments conducted at a 200 µm gap which concluded that study results were insensitive to gap dimension). The small gap was used to maximize
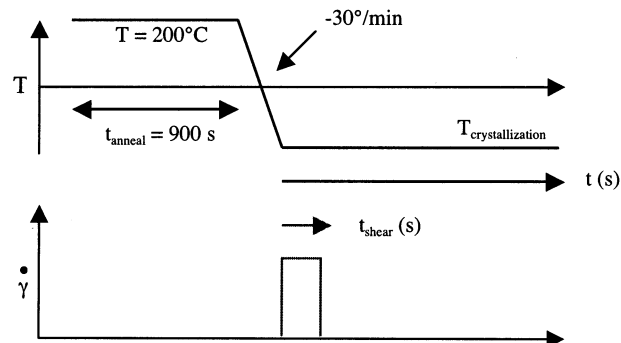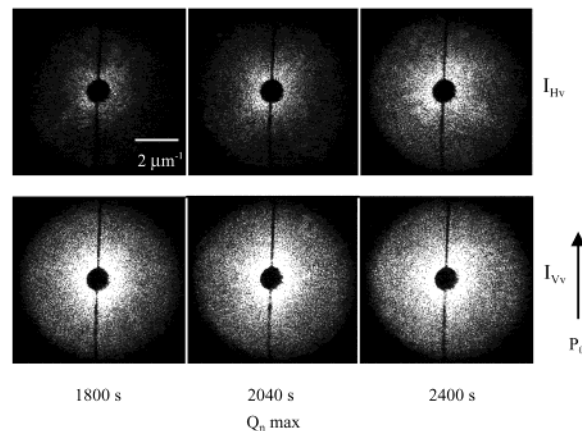
the applied shear rate and minimize the effect of multiple scattering in the late stages of the crystallization experiments. Shear rates within the range 1 s^{-1} < $\dot{\gamma}$ < 60 s^{-1} were studied.

After passing through a polarizer, scattered light was collimated by an aspheric condenser lens (diameter = 50 mm, $f = 37$ mm; Newport Inc., Irvine, CA). To block the primary beam illumination from the detector, a circular beam stop cut from a neutral density filter of optical density 5.0 (Newport Inc., Irvine, CA) was positioned behind the collimating lens. A pair of lenses (achromatic lens, diameter = 50.8 mm, $f = 250$ mm; achromatic lens, diameter = 12.7 mm, $f = 25.4$ mm; Newport Inc., Irvine, CA) separated by a distance equal to the sum of their focal lengths reduced the collimated path to the aperture of the detector. Detection of scattered light was by 12-bit cooled digital CCD camera (Sensicam VGA, 640 × 480 pixel resolution, and pixel size of 9.9 µm × 9.9 µm, Cooke Corp., Auburn Hills, MI). Images were acquired (IP lab software, Scanalytics Inc., Fairfax, VA) to a personal computer. The range of accessible scattering angles was determined by comparison of scattering from a dilute suspension of polystyrene latex (mean radius = 4.00 ± 0.29 µm) to the predictions of Mie scattering theory (Figure 3b). As demonstrated in Figure 3b, for the angular range 3° < θ < 15° we find acceptable agreement between theory and experiment.

Temperature and Shear Flow Protocol. The protocols for quiescent and shear flow experiments are shown schematically in Figure 4. The sample was annealed in the Linkham device at $T = 200$ °C for 15 min. The sample was cooled (without shearing) at 30 °C/min to the isothermal crystallization temperature, T_x (which was varied). At this time data were collected and (for flow-induced crystallization experiments) shear flow was applied.

SALS Data Analysis. Typical I_{Vv} and I_{Hv} scattering patterns are reported in Figure 5. The particular sample is a 2.0 wt % intercalated PP nanocomposite isothermally crystallized
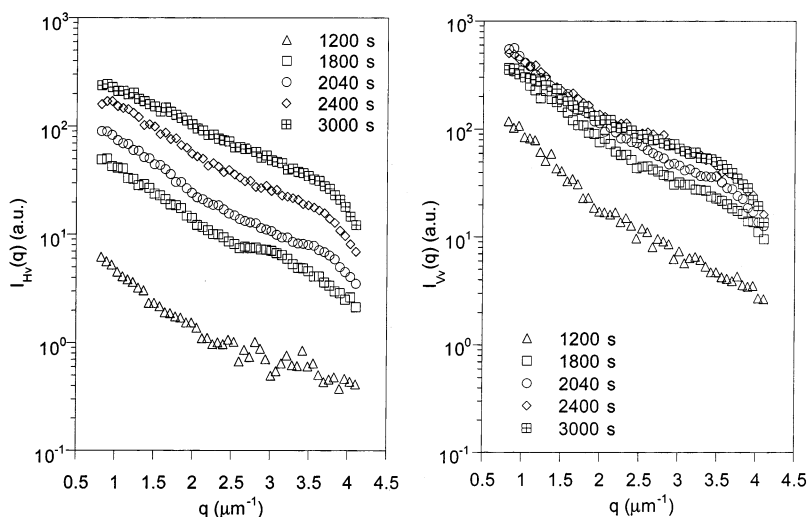
Figure 6. Measured I_{Hv} and I_{Vv} vs the scattering vector, q, extracted by azimuthal averaging of data such as Figure 5 at a number of different times during quiescent isothermal crystallization of the 2.0 wt % intercalated nanocomposite at $T = 142$ °C.

at $T = 142$ °C. Data at three different times are plotted. The scattering vector, $q = 4\pi n/\lambda \, \sin(\theta/2)$, increases with distance from the center of the image where n is the refractive index of the medium, λ is the wavelength of incident light, and θ is the scattering angle. Here I_{Vv} is the intensity of scattered light with polarization parallel to that of the incident beam, and I_{Hv} is the intensity of scattered light with polarization perpendicular to that of the incident beam. I_{Vv} is hereafter referred to as polarized or parallel-polarized scattering while I_{Hv} is called depolarized or cross-polarized scattering. Qualitatively, we find at early times that I_{Vv} increases while I_{Hv} remains small. I_{Vv} reaches a maximum at intermediate times while, later, I_{Hv} increases monotonically until the conclusion of the experiment. The theory of polarization-dependent light scattering due to Stein and co-workers[16,17] demonstrates that the depolarized component I_{Hv} is a function of spatial fluctuations in anisotropy of the refractive index, as is found, for example, in the growing lamellae of the crystalline regions. The polarized scattering component I_{Vv} consists of contributions both from refractive index anisotropy and from fluctuations in the isotropic refractive index due to the spatially varying density.

Interestingly, the radially symmetric scattering reported in Figure 5 is typical of all samples studied. (We observe four-lobe scattering patterns in I_{Hv} only at the longest times in a certain few nanocomposite samples.) Given that depolarized scattering with radial symmetry is a key prediction of the Stein and Wilson theory[17] of scattering from systems with random fluctuations in refractive index anisotropy, we analyze data with this formalism (as in refs 13–15). By azimuthally averaging of SALS data for rings of constant scattering vector, q, we compute the scattering vector dependent polarized, I_{Vv}-(q), and depolarized, $I_{Hv}(q)$, scattering intensity and report typical data in Figure 6. Note for all measurements we subtract the (small) melt state scattering (measured at $t = 0$) to compute $I_{Vv}(q)$ and $I_{Hv}(q)$. This correction removes the contributions of the amorphous polymer and clay scattering, which are small and not relevant to our objective of studying polymer crystallization. The subtraction is applied to all data reported in subsequent figures.

Characterization of Crystallization Times from Scattering Invariants. To develop characteristic light scattering measures of crystallization, we follow Koberstein et al.,[20] Okada et al.,[13] and Pogodina et al.[14,15] by computing the invariant measures Q_η and Q_δ that quantify density and orientation fluctuations, respectively. Here

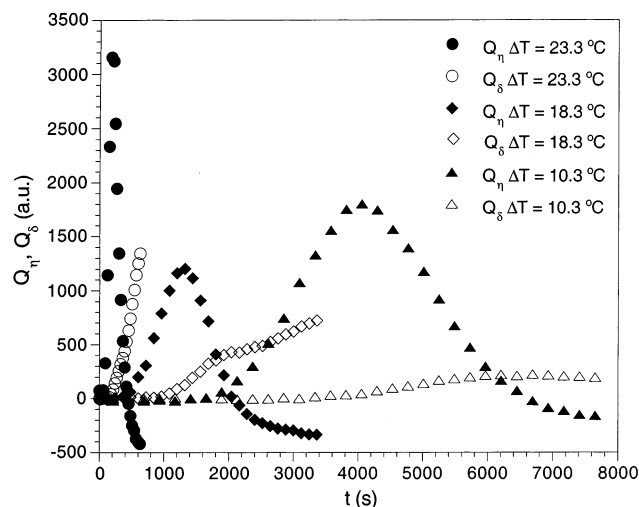$$Q_\eta = \int_{q_{min}}^{q_{max}} (I_{Vv} - \tfrac{4}{3} I_{Hv}) q^2 \, dq \qquad (1)$$

Figure 7. Time dependence of the invariant measures of density and orientation fluctuations, Q_η and Q_δ, computed according to eqs 1 and 2, for pure polypropylene at a number of different amounts of undercooling, ΔT. The maximum in Q_η is the characteristic light scattering crystallization time.

and

$$Q_\delta = \int_{q_{min}}^{q_{max}} I_{Hv} q^2 \, dq \qquad (2)$$

These quantities are related to integral measures of the total intensity of polarized and depolarized scattering at all angles. Here q_{max} and q_{min} are the limits probed by our small-angle light scattering device.

The time dependence of Q_η and Q_δ at three different degrees of undercooling for pure polypropylene is plotted in Figure 7. Results were computed by application of eqs 1 and 2 to the $I_{Vv}(q)$ and $I_{Hv}(q)$ obtained by azimuthal averaging of the raw scattering data. The maximum in Q_η is a characteristic light scattering time for crystallization.[13,15] It is thought to occur at a time when amorphous and crystalline regions are of equal volume fraction and thus density fluctuations are at a maximum.[13,15] These results are thus consistent with the earlier work of Okada et al.[13] and Pogodina et al.[15]

In Figure 8, the Q_η and Q_δ behavior of pure polypropylene and a 2.0 wt % intercalated polypropylene are compared at a constant degree of undercooling $\Delta T = 23.3$ °C. Because of the qualitatively similar behavior of its time-dependent Q_η and Q_δ, Figure 8 demonstrates that the approach of identifying the crystallization time from the maximum in Q_η is equally valid
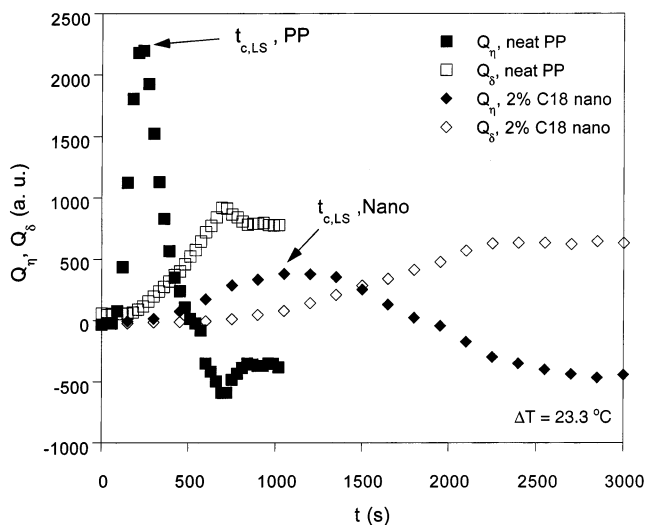
Figure 8. Comparison of the time dependence of the invariant measures of density and orientation fluctuations, Q_η and Q_δ, at fixed undercooling $\Delta T = 23.3$ °C for pure polypropylene and the 2.0 wt % polypropylene hybrid material.

for intercalated PP nanocomposites. Figure 8 also shows qualitatively that the intercalated PP nanocomposite crystallization, as characterized by light scattering, is retarded relative to pure PP. This result was systematically investigated, as reported later.

Note that the negative values of the invariant function Q_η observed in Figure 8 at long times occur for conditions where $I_{Vv}(q) \sim I_{Hv}(q)$. The negative values indicate a breakdown of the Koberstein et al. approach,[20] possibly due to the onset of multiple scattering. Although included for completeness, they do not affect the assignment of characteristic crystallization times that are the principal focus of the study.

Characterization of Isotropic Correlation Length by Debye−Bueche Analysis. Polypropylene crystallization scattering at early times has been found[13,15] to obey the Debye−Bueche scattering function:[18,19]

$$I(q) = \frac{A}{(1 + \xi^2 q^2)^2} \qquad (3)$$

where ξ is a characteristic correlation length and A is constant. If eq 3 is applied to I_{Vv} scattering at early times when $I_{Hv} \sim 0$, then ξ represents an isotropic correlation length. We verify that the scattering data at short times are well approximated by eq 3 (in agreement with refs 13 and 15) and thereby extract ξ as a function of degree of undercooling as shown in Figure 9 and its inset. The Debye−Bueche analysis was found to be equally applicable to studies of the intercalated polypropylene nanocomposite and the blend of polypropylene and compatibilizer (insets of Figure 12), and the time dependence of these correlation lengths is reported in the Results and Discussion section.

Polarized Optical Microscopy. To qualitatively confirm interesting features quantified by SALS, we conducted polarized light microscopy (10× objective, Olympus BX50, Olympus, NY, with images acquired from RTE/CCD-1300-Y/Hs digital camera, Roper Scientific, NJ) of certain specimens under quiescent and flow conditions using the previously described shear device. The materials, shear history, and thermal protocols were identical to those of the SALS studies. We emphasize the difference in length scales probed by SALS and polarized light microscopy: The former is sensitive to micronscale structure, while the latter probes structures on scales of approximately 100 μm.

Results and Discussion

Quiescent Crystallization. Isothermal light scattering crystallization times of intercalated polypropylene
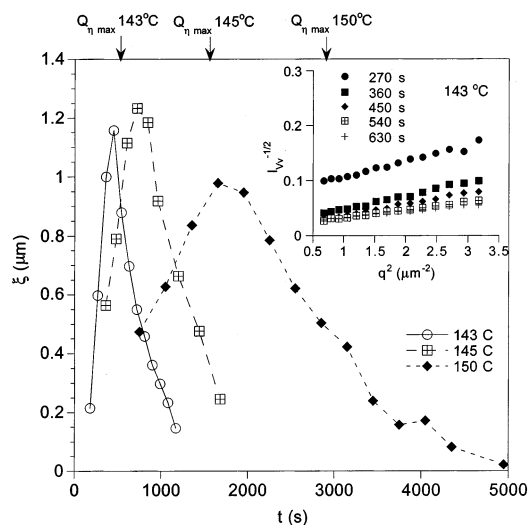

Figure 9. Time dependence of the isotropic correlation length, ξ, extracted by means of Debye−Bueche analysis (eq 3) for pure polypropylene at a number of different amounts of undercooling ΔT. For comparison, the corresponding characteristic crystallization times for Q_η are also shown. The inset plot shows sample Debye−Bueche plots used to extract ξ.
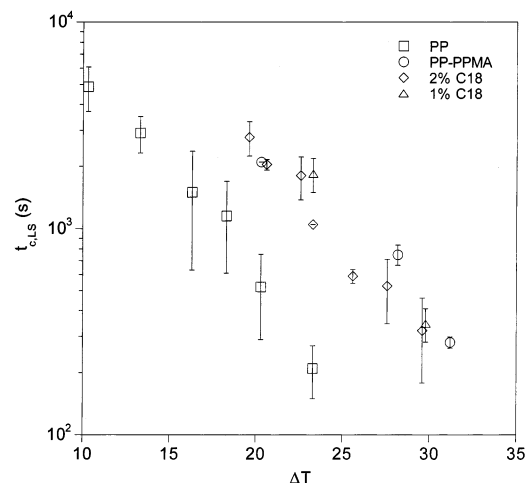

Figure 10. Characteristic light scattering crystallization time ($t_{C,LS}$) vs undercooling temperature (ΔT) for polypropylene and the 2.0 wt % intercalated nanocomposite. Data for the 7.28:1 blend of PP and PP−MA and a 1.0 wt % intercalated material are also shown for comparison.

nanocomposites with 2.0 wt % clay loading are shown in Figure 10 as a function of degree of undercooling, ΔT. To probe possible effects of sample heterogeneity on the crystallization kinetics, as many as six experiments were executed at each ΔT, and the resulting standard deviation was plotted. For comparison, experiments with pure polypropylene were also conducted. To resolve the possibly competing influences of the organophilic clay and the blended PP−MA compatibilizer, certain experiments with the 1.0 wt % clay nanocomposite and the PP/PP−MA blend were also conducted. (PP/PP−MA blend results are only reported for $\Delta T > 20$ °C. For smaller undercooling, a well-defined maximum in Q_η was not observed. We interpret this result to be consistent with the known differences between the crystallization behavior of polymer blends and single-component melts.[10])

Polypropylene Crystallization: Comparison to Prior Results. First, parenthetically, we note that the crystallization times of the pure polypropylene studied
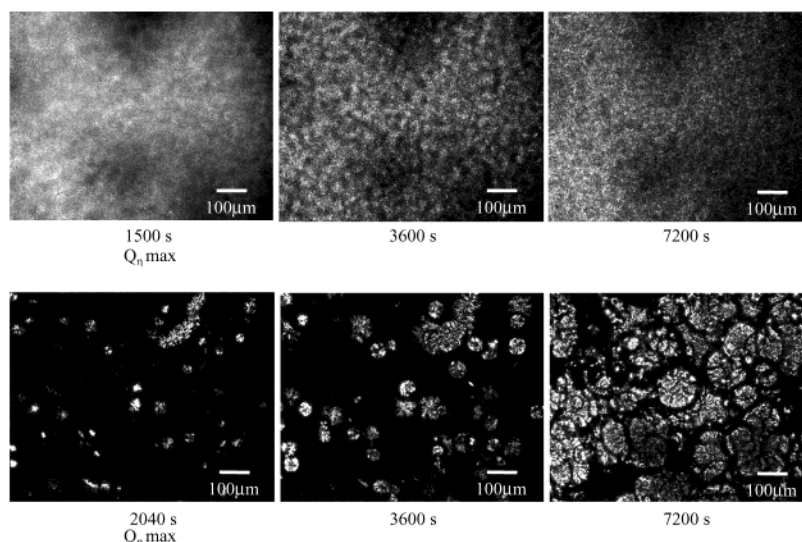
Figure 11. Comparison of polarizing light microscopy images for polypropylene (top) and the 2.0 wt % intercalated polypropylene nanocomposite (bottom) at different times for $\Delta T = 16.3$ °C ($T = 147$ °C). The acquisition time of the first images in each row corresponds to the characteristic light scattering crystallization times extracted from small-angle light scattering.
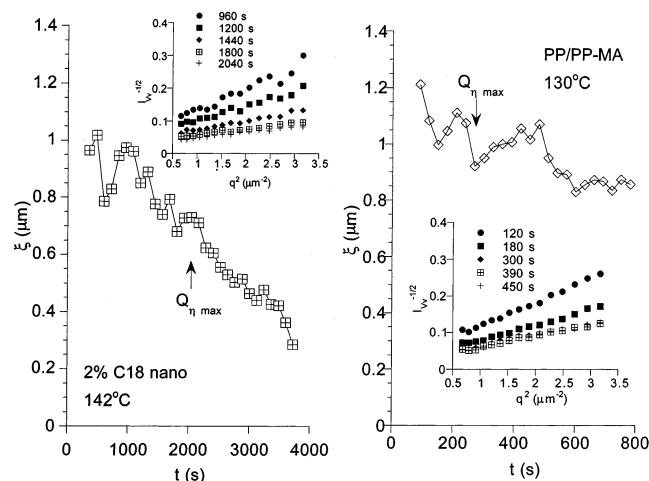

Figure 12. Isotropic correlation length, ξ, extracted from Debye−Bueche analysis for the intercalated PP nanocomposite and the blend of PP and the PP−MA compatibilizer. The experimental temperatures are given in the figures. For comparison, corresponding Q_η crystallization times are reported. The inset plots show sample Debye−Bueche plots used to extract ξ.

here are significantly smaller than reported for Pogodina et al.[15] for a different grade of isotactic polypropylene. Debye−Bueche analysis of the scattering data, polarizing light microscopy images, and melt-state viscosity measurements provide insight into this difference. Debye−Bueche correlation lengths (Figure 9) grow to the size of about 1 μm, in agreement with Pogodina et al.[15] However, the slopes of Figure 9 curves at early times yield characteristic growth rates that are qualitatively larger than Pogodina et al.[15] (data not shown). Polarizing light microscopy (Figure 11) reveals that the small crystallite morphology of our polypropylene grade grows quickly. This real space observation is consistent with a fast growth rate of micron scale structures (Figure 9) and fast light scattering crystallization kinetics (Figure 10). Finally, the zero-shear viscosity, η_0, of the isotactic polypropylene studied here at a reference temperature of 140 °C is 2700 Pa·s. This value is more than an order of magnitude lower than that of the material studied by Pogodina et al.

The variation in viscosity suggests that the molar mass distribution (or chain architecture) of the two polymers differs significantly, and such a difference affects observed crystallization times and growth rates.[10,41] (However, note that Acierno et al.[42] find little effect of molar mass on the early stage crystallization times characterized by small-amplitude oscillatory shear rheometry.) The presence of trace additives (nucleating agents in particular[13]) and differences in polymer tacticity[43] may also contribute to the difference between the crystallization of our grade and the Pogodina et al. grade of polypropylene. In particular, additives present in the polymer of the Okada et al. study[13] certainly contribute to the fact that their crystallization times are substantially faster than those reported here. Because Acierno et al.[42] find little effect of molar mass, we conclude that the explanation based on additives, perhaps related to the synthesis of the polymer, is the most likely possibility.

Quiescent Nanocomposite Crystallization. Next we compare the characteristic crystallization times of the polypropylene and intercalated nanocomposite. Contrary to earlier reports using differential scanning calorimetry,[5,44,45] the intercalated nanocomposite exhibits isothermal crystallization times that are retarded relative to pure polypropylene. Polarizing light microscopy (Figure 11) qualitatively confirms the difference in crystallization kinetics. Note furthermore in Figure 11 that the crystallite morphology of the polypropylene and intercalated nanocomposite are quite different. The polarizing light microscopy, which provides information on scales of ∼100 μm, is complementary to Figure 10 light scattering results, which probe smaller scales of ∼1 μm.

Further studies, also reported in Figure 10, found no significant difference among the crystallization times of 1.0 and 2.0 wt % clay/PP nanocomposite and the PP/PP−MA blend. Thus, we deduce that the retardation of the intercalated nanocomposite observed in Figure 10 is mediated by the use of the PP−MA compatibilizer.

Debye−Buche Analysis of Quiescent Crystallization. Debye−Bueche analysis reveals remarkable differences between the isotropic morphology of the intercalated nanocomposites (Figure 12) and pure

polypropylene (Figure 9). In Figure 12 we plot typical data; similar results at other degrees of undercooling were obtained. Recall from Figure 9 that at early times the pure polymer possesses a small isotropic correlation length that grows to a maximum value of approximately 1 μm within a period slightly less than the characteristic crystallization time extracted from the scattering invariant Q_η (as shown in Figure 7). From Figure 12 it is apparent that the intercalated polypropylene nanocomposite shows more complex behavior: even at early times, well before crystallization is detected by the invariant measure Q_η, the isotropic correlation length ξ is large—its value is approximately 1 μm. The magnitude of the correlation length then decreases monotonically over the course of the scattering experiment.

These results can be compared to the results of Debye–Bueche analysis for the PP/PP–MA blend, reported in Figure 12, which shows an isotropic correlation length ξ that is also initially large and then decreases by a modest amount over the course of the experiment. The result suggests that the blend is incompletely miscible at the temperatures at which the experiment was conducted. Our reasoning is that such a miscibility gap, if present, would yield a characteristic length scale in the blend that would be observable even at early times, prior to the development of significant crystal morphology. This characteristic scale would then mediate the subsequent growth of isotropic morphology during blend crystallization.

To understand the nanocomposite results of Figure 12, we recognize that the intercalated nanocomposite may possess two characteristic lengths that are absent from the pure polymer: (1) the size of the discotic clay or clay tactoids, which is certainly 1 μm or larger; (2) the domain structure size of the matrix blend of polypropylene and compatibilizer if the components are not fully miscible. In summary, at short times, when the magnitude of scattering is small because crystallite regions are only just beginning to form, Figure 12 demonstrates that isotropic features of size approximately 1 μm exist in polypropylene nanocomposites and are thereby available to influence the subsequent crystallization kinetics.

Comparison of Nanocomposite Quiescent Crystallization to Prior Differential Scanning Calorimetry. A discrepancy exists between this study that observed retarded kinetics for PP nanocomposites and previous differential scanning calorimetry (DSC) characterizations of crystallization in polypropylene nanocomposites that reported accelerated kinetics.[5,44,45] This discrepancy is not directly linked to the presence of compatibilizer, since the acceleration has been observed for both uncompatiblized[44] and compatibilized[5,45] nanocomposites. A possible origin of the discrepancy is the difference in experiment (light scattering vs DSC). However, we conducted isothermal DSC studies and found retarded kinetics even with that method. In addition, good qualitative correspondence between DSC and light scattering results has previously been reported.[15]

Alternatively, we reason that there must be some important difference between the clay or compatibilizer properties of the materials studied here and those studied in the earlier reports. Interestingly, we note that the recent finding of Maiti et al.[46] (that the addition of organophilic clay to compatibilizer does not affect crystallization times) is consistent with our finding that
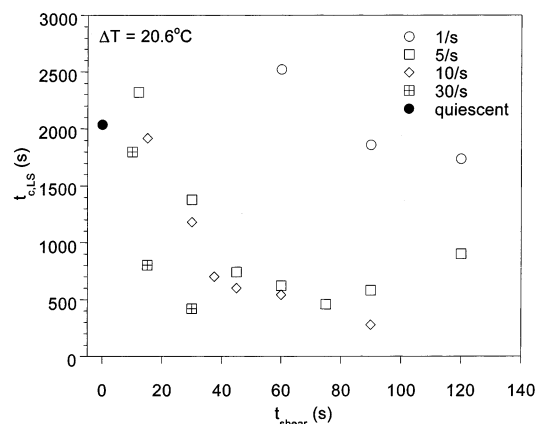

Figure 13. Dependence of the 2.0 wt % intercalated nanocomposite characteristic light scattering crystallization time $t_{C,LS}$ on shear time at a number of shear rates for undercooling ΔT = 20.6 °C.

the compatibilizer dominates the nanocomposite quiescent crystallization process. We also note the earlier literature is not entirely definitive on the question of crystallization kinetics of polypropylene nanocomposites. First, Svoboda et al.[5] found accelerated crystallization kinetics with DSC and retarded spherulite growth rates with optical microscopy. Second, Jimenez et al. found both acceleration and retardation of crystallization kinetics for poly(ϵ-caprolactone)–clay hybrid materials.[47]

The observation that PP nanocomposite crystallization times correlate closely with those for the PP/PP–MA blend suggests the possibility that the polymer matrix of the intercalated nanocomposites is truly a blend of PP and PP–MA. That is, the PP–MA compatibilizer cannot be largely sequestered in the clay gallery regions, because the early stage, micron scale crystal kinetics of the intercalated nanocomposite are remarkably similar to those of a simple blend of PP/PP–MA. It has been suggested that a melt homogeneous matrix of PP and PP–MA is advantageous to the development of material property enhancement[4] because miscibility promotes clay dispersion. Here we find an additional effect of the two-component system: it significantly retards crystallization kinetics on the micron scale. This retardation, which leads to different crystallite morphology, is certainly relevant to understanding the solid-state material properties of compatibilized polymer/clay nanocomposites.

Flow-Induced Crystallization. As described by Liedauer et al.,[29,30] we systematically study the effect of shear flow on isothermal polymer crystallization by applying a short episode of deformation followed by isothermal crystallization. The time during which the flow is applied is less than 10% of the characteristic time for crystallization and the shear flow can be viewed as a preconditioning step that affects the subsequent quiescent crystallization process. This shear history is a good model of industrial processes such as injection molding, wherein crystallization occurs quiescently after the polymer is injected into the mold. As depicted in Figure 4, we apply the shear deformation to the undercooled melt to eliminate any possible effect of the ~100 s waiting time required for the thermal quench.

Results of experiments at a number of shear rates and shear times for the 2.0 wt % nanocomposite are plotted in Figure 13. As for quiescent studies, the datum points are averages of up to six experiments. The crystalliza-
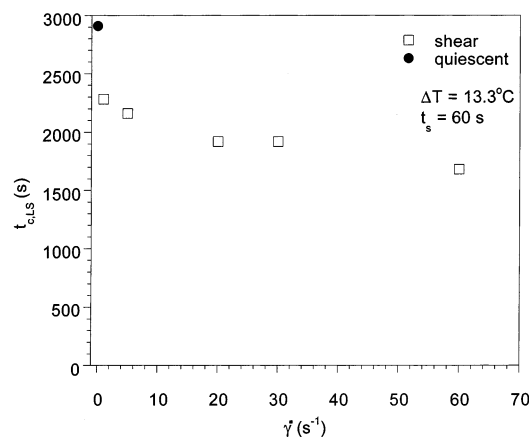
Figure 14. Shear flow-induced crystallization of polypropylene at $\Delta T = 13.3$ °C at fixed shear time for a number of shear rates. The amount of undercooling was chosen so that the quiescent crystallization times of the PP matched that of the 2.0 wt % intercalated nanocomposite reported in Figure 13.
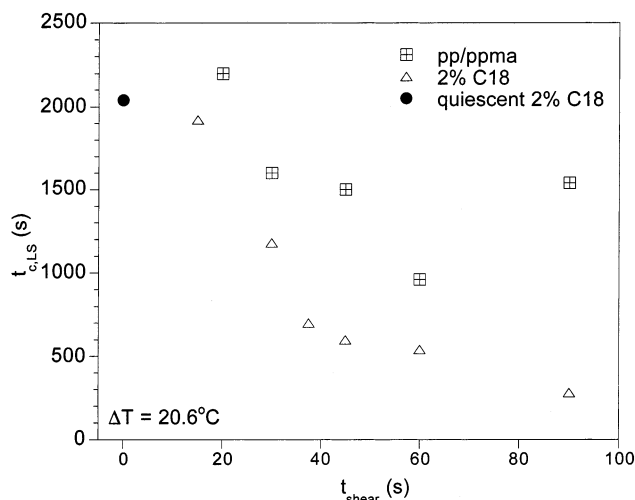

Figure 15. Comparison of the flow-induced crystallization behavior of the 2.0 wt % intercalated nanocomposite and the blend of PP and the PP–MA compatibilizer at $\Delta T = 20.6$ °C and shear rate of 10 s^{-1}.

tion times were extracted according to the data analysis methods described previously, and the standard deviation of measurements was found to be comparable to those reported in Figure 10. We observed radially symmetric scattering patterns under all conditions. Figure 13 reports a major finding of our study, which is that the effect of flow on the light scattering crystallization times of PP/nanocomposites is significant. The amount by which crystallization is accelerated by flow increases with both shear rate and shear time. In the remainder of this paper we describe experiments designed to understand the magnitude, scaling, and origin of this effect.

Comparison of Flow-Induced Nanocomposite Crystallization with Effect of Flow on Pure Polypropylene. For purposes of comparison to the intercalated nanocomposite data, we tested pure polypropylene at $\Delta T = 13.3$ °C. This undercooling, different than the conditions for Figure 13 experiments ($\Delta T = 20.6$ °C), was selected so that the pure polypropylene quiescent crystallization time was approximately equal to that of the nanocomposite experiments reported in Figure 13. At such conditions, the effect of shear flow on polypropylene crystallization is modest, as shown in Figure 14. For example, comparison of data at approximately equivalent shear rates and times shows that when the maximum effect of flow on the nanocomposite crystallization is observed, the effect of flow on polypropylene is 5 times smaller than for the nanocomposite.

The effect of flow on polypropylene observed here may be compared to the recent flow-induced crystallization studies of Pogodina et al.,[14] Kumaraswamy et al.,[23,24] Seki et al.,[27] and Liedauer et al.[30] These studies reported significant flow effects on crystallization, anisotropic scattering, and oriented structure. The relationship between our results and those of Pogodina et al.[14] for different grades of polypropylene are of particular interest since they were conducted in a similar device at similar rates of deformation. Yet, we observed only isotropic crystal morphology, while Pogodina et al.[14] observed anisotropic crystal morphology at high rates of deformation ($\dot{\gamma} = 10$ s^{-1}). To further address this issue, we tested two additional grades of isotactic polypropylene (Achieve 3854, Exxon Mobil, Houston, TX, and Pro-fax 6523, Basell, Wilmington, DE) at rates of deformation comparable to those of Pogodina et al.[14] These materials displayed isotropic structure at the

shear rates studied. Our observations are consistent with Liedauer et al.[30] and Seki et al.[27] Liedauer et al.[30] reported that upon increasing rate of deformation the polymer morphology changes from coarse-grained spherulitic structure to fine-grained spherulitic structure (weak shear treatment) and then to a structure that is highly oriented (strong shear treatment). In addition, Seki et al.[27] report that although weak shear treatment does not yield oriented crystallization, it does accelerate crystallization kinetics relative to quiescent conditions. The conditions of our study for pure polypropylene, which demonstrated a modest effect of shear on crystallization, radially symmetric scattering, and an absence of oriented structures in polarized microscopy, are thus consistent with weak shear treatment. Seki et al.[27] have linked this regime to the average local stress and orientation of polymer chains.

Comparison of Figures 13 and 14 suggests that nanocomposites experience significant acceleration of crystallization at shear rates and times that induce only moderate effects in polypropylene. To understand the origin of the difference between flow-induced crystallization in polypropylene and intercalated nanocomposites, we report in Figure 15 a comparison between flow-induced effects in the nanocomposite and in the PP/PP–MA blend. Figure 15 demonstrates that flow does affect the blend crystallization kinetics, but not to as great a degree as for the nanocomposite. Thus, on the basis of Figure 15, it appears that a role for the compatibilizer in mediating the intercalated nanocomposite flow-induced crystallization cannot be ruled out.

To learn whether a link exists between flow-induced acceleration of crystallization and oriented morphology in intercalated nanocomposites, we observed crystallite morphology by polarizing microscopy. The results, reported in Figure 16, demonstrate an absence of oriented structures. Consistent with this finding, light scattering patterns were also isotropic. Since it is believed that the mechanism for enhancement of crystallization kinetics when oriented structures are absent is the increase in the number of point nuclei,[27] we hypothesize that the heterogeneity of the intercalated nanocomposites is the origin of the behavior observed in Figures 13 and 15. The heterogeneity, induced by both the clay and blend components, may facilitate the flow-induced formation
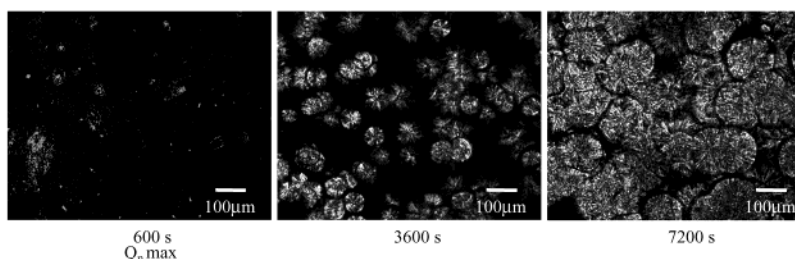
Figure 16. Polarizing light microscopy of the 2.0 wt % intercalated nanocomposite after shear flow at rate 10 s^{-1} and time 60 s at $T = 142$ °C ($\Delta T = 20.6$ °C). The conditions are those for which flow-induced crystallization effects were measured by light scattering. Consistent with the light scattering, oriented structures are absent from the nanocomposite.
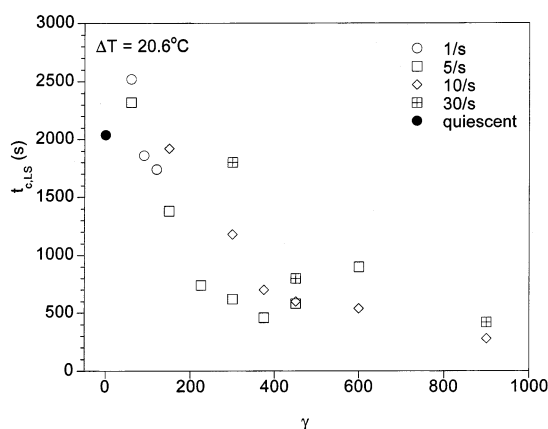

Figure 17. Flow-induced crystallization results of Figure 13 for the 2.0 wt % intercalated nanocomposite now plotted vs the applied strain.

of point nuclei by increasing the average local stress and orientation of polymer molecules.

In Figure 17, we test the hypothesis that the observed strain rate and shear time dependence of Figure 13 is a unique function of the applied total strain. It appears that the intercalated nanocomposite response is better correlated by strain (Figure 17) than by shear time (Figure 13). In addition, the scaling of the effect for nanocomposites observed here differs substantially from the dependence reported for polypropylene by Liedauer et al.[29] Taken together, the results of Figures 11, 16, and 17 point to a mechanism for flow-induced crystallization of intercalated nanocomposites that involves an enhancement in the number of point nuclei due to an increase in the local stress and orientation of the matrix polypropylene that is induced by the heterogeneous clay/blend morphology. Real space imaging to probe the relative location of the clay platelets and the growing polymer crystallites is warranted to address this hypothesis.

Conclusions

This study has identified four particular ways in which the crystallization kinetics and morphology of intercalated polypropylene nanocomposites differ from that of pure polypropylene: (1) The use of the PP−MA compatibilizer contributes to the retardation of the quiescent isothermal crystallization kinetics of the intercalated nanocomposites relative to polypropylene. (2) The time dependence of the isotropic correlation length of the nanocomposite during crystallization obeys behavior different than polypropylene due to the effects of the dispersed clay and/or compatibilizer. (3) The application of shear flow accelerates the crystallization kinetics of the intercalated nanocomposites under con-

ditions at which the polypropylene shows small flow-induced effects. (4) The mechanism that generates the effect of flow on crystallization for nanocomposites operates in a regime where the resulting polymer morphology is isotropic, thereby suggesting that the heterogeneity of the clay/blend morphology affects flow-induced crystallization through its influence on the local stress and orientation of the matrix polypropylene.

References and Notes

(1) Vaia, R.; Giannelis, E. P. *MRS Bull.* **2001**, *26*, 394−401.
(2) Kojima, Y.; Usuki, A.; Kawasumi, M.; Okada, A.; Fukushima, Y.; Kurauchi, T.; Kamigaito, O. *J. Mater. Res.* **1993**, *8*, 1185−1189.
(3) Fornes, T. D.; Yoon, P. J.; Keskkula, H.; Paul, D. R. *Polymer* **2001**, *42*, 9929−9940.
(4) Kawasumi, M.; Hasegawa, N.; Kato, M.; Usuki, A.; Okada, A. *Macromolecules* **1997**, *30*, 6333−6338.
(5) Svoboda, P.; Zeng, C.; Wang, H.; Lee, J.; Tomasko, D. L. *J. Appl. Polym. Sci.* **2002**, *85*, 1562−1570.
(6) Brune, D. A.; Bicerano, J. *Polymer* **2002**, *43*, 369−387.
(7) Ji, X. L.; Jing, K. J.; Jiang, W.; Jiang, B. Z. *Polym. Eng. Sci.* **2002**, *42*, 983−993.
(8) Lincoln, D. M.; Vaia, R. A.; Wang, Z.-G.; Hsiao, B. S.; Krishnamoorti, R. *Polymer* **2001**, *42*, 9975−9985.
(9) Lincoln, D. M.; Vaia, R. A.; Wang, Z.-G.; Hsiao, B. S. *Polymer* **2001**, *42*, 1621−1631.
(10) Schultz, J. M. *Polymer Crystallization: The Development of Crystalline Order in Thermoplastic Polymers*; American Chemical Society: Washington, DC, 2001.
(11) Pogodina, N. V.; Winter, H. H. *Macromolecules* **1998**, *31*, 8164−8172.
(12) Wang, Z.-G.; Hsiao, B. S.; Sirota, E. B.; Agarwal, P.; Srinivas, S. *Macromolecules* **2000**, *33*, 978−989.
(13) Okada, T.; Saito, H.; Inoue, T. *Macromolecules* **1992**, *25*, 1908−1911.
(14) Pogodina, N. V.; Lavrenko, V. P.; Srinivas, S.; Winter, H. H. *Polymer* **2001**, *42*, 9031−9043.
(15) Pogodina, N. V.; Siddiquee, S. K.; van Egmond, J. W.; Winter, H. H. *Macromolecules* **1999**, *32*, 1167−1174.
(16) Stein, R. S.; Rhodes, M. B. *J. Appl. Phys.* **1960**, *31*, 1873−1884.
(17) Stein, R. S.; Wilson, P. R. *J. Appl. Phys.* **1962**, *33*, 1914−1922.
(18) Debye, P.; Anderson, H. R.; Brumberger, H. *J. Appl. Phys.* **1957**, *28*, 679−683.
(19) Debye, P.; Bueche, A. M. *J. Appl. Phys.* **1949**, *20*, 518−525.
(20) Koberstein, J.; Russell, T. P.; Stein, R. S. *J. Polym. Sci., Part B: Polym. Phys.* **1979**, *17*, 1719−1730.
(21) Yoon, D. Y.; Stein, R. S. *J. Polym. Sci.* **1974**, *12*, 735−761.
(22) Kumaraswamy, G.; Kornfield, J. A.; Yeh, F.; Hsiao, B. S. *Macromolecules* **2002**, *35*, 1762−1769.
(23) Kumaraswamy, G.; Verma, R. K.; Issaian, A. M.; Wang, P.; Kornfield, J. A.; Yeh, F.; Hsiao, B. S.; Olley, R. H. *Polymer* **2000**, *41*, 8931−8940.

(24) Kumaraswamy, G.; Issaian, A. M.; Kornfield, J. A. *Macromolecules* **1999**, *32*, 7537−7547.

(25) Kumaraswamy, G.; Verma, R. K.; Kornfield, J. A. *Rev. Sci. Instrum.* **1999**, *70*, 2097−2104.

(26) Somani, R. H.; Hsiao, B. S.; Nogales, A.; Srinivas, S.; Tsou, A. H.; Sics, I.; Balta-Calleja, F. J.; Ezquerra, T. A. *Macromolecules* **2000**, *33*, 9385−9394.

(27) Seki, M.; Thurman, D. W.; Oberhauser, J. P.; Kornfield, J. A. *Macromolecules* **2002**, *35*, 2583−2594.

(28) Nogales, A.; Hsiao, B. S.; Somani, R. H.; Srinivas, S.; Tsou, A. H.; Balta-Calleja, F. J.; Ezquerra, T. A. *Polymer* **2001**, *42*, 5247−5256.

(29) Liedauer, S.; Eder, G.; Janeschitz-Kriegl, H.; Jerschow, P.; Geymayer, W.; Ingolic, E. *Int. Polym. Process.* **1993**, *8*, 236−244.

(30) Liedauer, S.; Eder, G.; Janeschitz-Kriegl, H. *Int. Polym. Process.* **1995**, *10*, 243−250.

(31) Duplay, C.; Monasse, B.; Haudin, J.-M.; Costa, J.-L. *Polym. Int.* **1999**, *48*, 320−326.

(32) Eder, G.; Janeschitz-Kriegl, H.; Liedauer, S. *Prog. Polym. Sci.* **1990**, *15*, 629−714.

(33) McHugh, A. J.; Guy, R. K.; Tree, D. A. *Colloid Polym. Sci.* **1993**, *271*, 629−645.

(34) Somani, R. H.; Yang, L.; Hsiao, B. S. *Physica A* **2002**, *304*, 145−157.

(35) Medellin-Rodriguez, F. J.; Burger, C.; Hsiao, B. S.; Chu, B.; Vaia, R.; Phillips, S. *Polymer* **2001**, *42*, 9015−9023.

(36) Okamoto, M.; Nam, P. H.; Maiti, P.; Kotaka, T.; Hasegawa, N.; Usuki, A. *Nano Lett.* **2001**, *1*, 295−298.

(37) Okamoto, M.; Nam, P. H.; Maiti, P.; Kotaka, T.; Nakayama, T.; Takada, M.; Ohshima, M.; Usuki, A.; Hasegawa, N.; Okamoto, H. *Nano Lett.* **2001**, *1*, 503−505.

(38) Solomon, M. J.; Almusallam, A. S.; Seefeldt, K. F.; Somwangthanaroj, A.; Varadan, P. *Macromolecules* **2001**, *34*, 1864−1872.

(39) Cho, K.; Li, F.; Choi, J. *Polymer* **1998**, *1999*, 1719−1729.

(40) Varadan, P.; Solomon, M. J. *Langmuir* **2001**, *17*, 2918−2929.

(41) Isayev, A. I.; Catignani, B. F. *Polym. Eng. Sci.* **1997**, *37*, 1526−1539.

(42) Acierno, S.; Grizzuti, N.; Winter, H. H. *Macromolecules* **2002**, *35*, 5043−5048.

(43) Lu, H.; Qiao, J.; Xu, Y.; Yang, Y. *J. Appl. Polym. Sci.* **2002**, *85*, 333−341.

(44) Ma, J.; Zhang, S.; Qi, A.; Li, G.; Hu, Y. *J. Appl. Polym. Sci.* **2002**, *83*, 1978−1985.

(45) Hambir, S.; Bulakh, N.; Kodgire, P.; Kalgaonkar, R.; Jog, J. P. *J. Polym. Sci., Part B: Polym. Phys.* **2001**, *39*, 446−450.

(46) Maiti, P.; Nam, P. H.; Okamoto, M.; Hasegawa, N.; Usuki, A. *Macromolecules* **2002**, *35*, 2042−2049.

(47) Jimenez, G.; Ogata, N.; Kawai, H.; Ogihara, T. *J. Appl. Polym. Sci.* **1997**, *64*, 2211−2220.